Lithium chloride corrects weakness and myopathology in a preclinical model of LGMD1D

Andrew R. Findlay, MD,* Rocio Bengoechea, PhD,* Sara K. Pittman, BS, Tsui-Fen Chou, PhD,
Heather L. True, PhD, and Conrad C. Weihl, MD, PhD

Correspondence
Dr. Findlay
arfindlay@wustl.edu

Abstract

Objective
To understand DNAJB6's function in skeletal muscle and identify therapeutic targets for limb-girdle muscular dystrophy 1D (LGMD1D).

Methods
DNAJB6 knockout (KO) myoblasts were generated with Crispr/cas9 technology, and differentially accumulated proteins were identified using stable isotope labeling, followed by quantitative mass spectrometry. Cultured KO myotubes and mouse muscle from DNAJB6b-WT or DNAJB6b-F93L mice were analyzed using histochemistry, immunohistochemistry, and immunoblot. Mouse functional strength measures included forelimb grip strength and inverted wire hang.

Results
DNAJB6 inactivation leads to the accumulation of sarcomeric proteins and hypertrophic myotubes with an enhanced fusion index. The increased fusion in DNAJB6 KO myotubes correlates with diminished glycogen synthase kinase-β (GSK3β) activity. In contrast, LGMD1D mutations in *DNAJB6* enhance GSK3β activation and suppress β-catenin and NFAT3c signaling. GSK3β inhibition with lithium chloride improves muscle size and strength in an LGMD1D preclinical mouse model.

Conclusions
Our results suggest that DNAJB6 facilitates protein quality control and negatively regulates myogenic signaling. In addition, LGMD1D-associated *DNAJB6* mutations inhibit myogenic signaling through augmented GSK3β activity. GSK3β inhibition with lithium chloride may be a therapeutic option in LGMD1D.

---

*These authors contributed equally to the manuscript.

From the Washington University School of Medicine (A.R.F., R.B., S.K.P., H.L.T., C.C.W); Department of Neurology (A.R.F., R.B., S.K.P., C.C.W), Hope Center for Neurological Diseases, St. Louis, MO; Harbor-UCLA Medical Center (T.-F.C.), Department of Pediatrics, Division of Medical Genetics, Torrance, CA; Department of Cell Biology and Physiology (H.L.T.), Saint Louis, MO.

Glossary

CSA = cross-sectional area; **GFP** = green fluorescent protein; **GO** = Gene Ontology; **GSK3β** = glycogen synthase kinase-β; **HSP** = heat shock protein; **KO** = knockout; **LGMD1D** = limb-girdle muscular dystrophy 1D; **LC-MS/MS** = Liquid chromatography with tandem mass spectrometry; **NFATc3** = nuclear factor of activated T cells cytoplasmic 3; **PBS** = phosphate-buffered saline; **SILAC** = stable isotope labeling with amino acids in cell culture; **WT** = wild type.

Protein chaperones, or heat shock proteins (HSPs), are increasingly recognized as critical for skeletal muscle health.[1] Recently, mutations in *DNAJB6*, an HSP40 co-chaperone, were identified to cause limb-girdle muscular dystrophy 1D (LGMD1D), also known as LGMD D1 DNAJB6-related, a childhood- or adult-onset, dominantly inherited, progressive myopathy with vacuolar and aggregate myopathology.[2–5] *DNAJB6* is ubiquitously transcribed and mediates proper folding and disaggregation of proteins by HSP70.[6,7] It has 2 isoforms: DNAJB6a, which localizes to the nucleus, and DNAJB6b, which localizes diffusely.[4,8] In skeletal muscle, DNAJB6b localizes to the Z disc and is thought to be the isoform responsible for disease pathogenesis of LGMD1D.[4,8] LGMD1D mutations in *DNAJB6* reside within the G/F domain, a region important for client protein handling.[4,8] DNAJB6's role in normal muscle and the pathomechanism of disease mutations is unknown.

In addition to its role in protein homeostasis, DNAJB6 also acts as a tumor suppressor through its interaction with glycogen synthase kinase-β (GSK3β).[9,10] GSK3β activity is dependent on DNAJB6 chaperoning a multiprotein complex to maintain its dephosphorylated (active) state.[10] Active GSK3β negatively regulates several myogenic signaling pathways, including β-catenin and nuclear factor of activated T cells cytoplasmic 3 (NFATc3) signaling.[10–15] DNAJB6 has also been shown to directly interact with and inhibit NFATc3 transcriptional activity by recruiting class II histone deacetylases.[16] In this study, we explored DNAJB6's role in skeletal muscle and its impact on myogenesis and related signaling pathways. We also investigated *DNAJB6* disease mutation's impact on these pathways and their contribution to LGMD1D pathogenesis.

Methods

Generation of DNAJB6 knockout (KO) C2C12 myoblasts

DNAJB6 KO C2C12 cells were generated using 2 guide RNAs targeting 2 introns of *DNAJB6* to generate a 5.5-kb out-of-frame deletion (figure e-1A, links.lww.com/NXG/A147). We used this strategy to avoid modifying other *DNAJ* genes. Clones were screened for homozygosity of the 5.5-kb deletion via sequencing (figure e-1B). Absence of DNAJB6 protein expression was confirmed via western blot (figure 1A).

Antibodies

Antibodies used were the following: anti-rabbit GAPDH (Cell Signaling, 2118), anti-rabbit desmin (Abcam, ab8592), anti-rabbit DNAJB6 (Abcam, ab75196), anti-rabbit αβ-crystallin (Enzo, ADI-SPA-223), anti-mouse hnRNPA2/B1 (Sigma, R4653), anti-rabbit alpha-actinin (Abcam ab68167), anti-mouse keratin 18 (Abcam, ab668), anti-rabbit GSK3β-P(ser-9) (Cell Signaling, 9336), anti-rabbit GSK3β (Cell Signaling, 9315), anti-goat FHL-1 (Abcam ab23937), and anti-mouse myosin (Sigma-Aldrich, M1570). Secondary antibodies include anti-mouse HRP (Pierce), anti-rabbit HRP (Cell Signaling), anti-goat HRP (Santa Cruz), and anti-mouse AlexaFluor (488).

Western blot

Muscle tissues and cultured cells were homogenized using RIPA lysis buffer (50 mM Tris-HCl, pH 7.4, 150 mM NaCl, 1% NP-40, 0.25% Na-deoxycholate and 1 mM EDTA) supplemented with protease inhibitor cocktail (Sigma-Aldrich), and lysates were centrifuged at 21380*g* for 10 minutes. Protein concentrations were determined using a BCA protein assay kit (Thermo Fisher Scientific). Aliquots of lysates were solubilized in Laemmli buffer, and equal amounts of proteins were separated on 12% sodium dodecyl sulfate polyacrylamide gels. Proteins were transferred to nitrocellulose membrane, and the membrane was blocked with 5% nonfat dry milk in phosphate-buffered saline (PBS) with 0.1% Tween-20 for 1 hour. The membrane was then incubated with primary antibody, in 5% nonfat dry milk overnight at 4°C, and then secondary antibody conjugated with horseradish peroxidase. Enhanced chemiluminescence (GH Healthcare, UK) was used for protein detection. Immunoblots were obtained using the G:BoxChemi XT4, Genesys Version 1.1.2.0 (Syngene). Densitometry was measured with ImageJ software (NIH).

Cell culture

HeLa cells were maintained in Dulbecco's Modified Eagle medium (DMEM, Gibco #11965-084), 10% fetal bovine serum (FBS, Atlanta Biologicals #S10350H), and 50 μg/mL penicillin and streptomycin (P/S, Sigma #P4333) at 37°C with 5% CO2. C2C12 cells were maintained in proliferation media (DMEM with 20% FBS, 50 μg/mL P/S) and switched to differentiation media (DMEM with 2% horse serum, 50 μg/mL P/S) to form myotubes. Transfection of cells was performed with Lipofectamine 2000 (Life Technologies #11668019) according to the manufacturer's instruction.

Plasmid construction

Mammalian constructs of DNAJB6b were cloned using site-directed mutagenesis, digested with HindIII/XhoI, and ligated into vector pcDNA3.1 containing a green fluorescent protein (GFP) tag. DNAJB6b F89I and P96R mutations were generated with the Quik Change Mutagenesis Kit (Agilent Technologies #200517).

Immunofluorescence

C2C12 cells were grown, stained, and imaged directly on cell culture plastic. Cells were washed 3 times with PBS, fixed in 4% PFA for 10 minutes, permeabilized with 0.1% Triton X-100 in PBS for 10 minutes, and then blocked with 3% BSA in PBS for 30 minutes to 1 hour at room temperature. Cells were stained with primary antibody (anti-mouse myosin) at 4°C overnight, followed by washing 3 times with PBS. Cells were incubated with Alexa 488 Fluor-conjugated secondary antibody at RT for 1 hour and mounted with Mowiol media containing 4′,6-diamidino-2-phenylindole. C2C12 differentiation experiments were performed in triplicate. Fusion index was determined as a ratio of nuclei number within multinucleated myosin-positive myotubes to the total number of nuclei. Nuclei were counted from 10 random fields taken with 10× objective equipped in a NIKON Eclipse 80i fluorescence microscope. Myosin stained myotubes with irregular staining pattern were counted and divided by the total number of myosin-positive myotubes to quantify the percent of myotubes with irregular myosin staining.

Electron microscopy

C2C12 cells were differentiated for 6 days, rinsed briefly in PBS, and fixed immediately with Karnovsky fixative at 4°C for 24 hours. Fixed myotubes were embedded in plastic and sectioned for imaging with a JEOL JEM-1400 Plus 120 kV Transmission Electron Microscope equipped with an AMT XR111 high-speed $4 \text{ k} \times 2 \text{ k}$ pixel phosphor-scintillated 12-bit charge coupled device camera.

Stable isotope labeling by amino acids and mass spectrometry

For "forward" stable isotope labeling with amino acids in cell culture (SILAC) experiments, KO C2C12 cells were cultured in "heavy" media in which Arg and Lys were replaced by $^{13}C_6$-Arg and $^{13}C_6$, $^{15}N_2$-Lys, whereas C2C12 DNAJB6 wild-type (WT) cells were grown in "light" media containing $^{12}C_6$-Arg and $^{12}C_6$, $^{14}N_2$-Lys (Thermo Fisher). For "reverse" experiments, DNAJB6 KO C2C12 cells were grown in "light" media and WT C2C12 cells were grown in "heavy" media. Two biological replicates were used for each condition. Myoblasts were passaged 6 times to allow for sufficient incorporation of label. For mass spectrometry analyses, we used the same methodology as the one used in previous studies with minor modification.[17,18] Briefly, total cell lysate was generated using 9 M Urea in 20 mM HEPES, pH 8.0 containing protease inhibitor and phosphatase inhibitor tablets. Equal amount (0.3 mg) for each cell type was mixed and digested using Lys-C and trypsin digestion protocol as described.[17,18] The peptides were loaded onto an Easy Nano-LC Q-Exactive Orbitrap, and the peak lists were generated using Proteome Discoverer software (Thermo Fisher Scientific).[18] Only proteins that were present in all biological replicates in both forward and reverse SILAC experiments were considered for further data analysis. Proteins were considered increased in DNAJB6 KO C2C12 cells if there was at least a 1.5-fold change in forward KO/WT experiments and a 0.6-fold change in reverse WT/KO experiments. Proteins were considered decreased in DNAJB6 KO C2C12 cells if there was at least a 0.6-fold change in forward KO/WT experiments and a 1.5-fold change in reverse WT/KO experiments.

Ontological analysis

All differentially expressed proteins were classified broadly into several catalogs according to the Gene Ontology (GO) annotation (geneontology.org). Overrepresentation analyses of GO terms, including biological process, molecular function, and cellular component, were performed using the ConsensusPathDB-human database system (cpdb.molgen.mpg.de/CPDB), which is a molecular functional interaction database. All proteins detected in SILAC experiments were used as background for comparison. The GO level 2 and 3 categories and a p value cutoff of 0.01 were selected.

Luciferase assays

C2C12 myoblasts were transfected with 20 ng Renilla control reporter (pRL-TK) and either 1 μg of the β-catenin luciferase reporter (TOPflash, Addgene plasmid #12456) or 1 μg of an NFAT-sensitive luciferase reporter (pGL3-NFAT luciferase, Addgene plasmid #17870).

HeLa cells were transfected with 0.5 μg of GFP control or GFP-tagged DNAJB6b construct, 20 ng Renilla control reporter, and either 0.5 μg of the β-catenin luciferase reporter or 0.5 μg of an NFAT-sensitive luciferase reporter. For β-catenin luciferase experiments, HeLa cells were treated with 20 mM lithium chloride (LiCl) (Sigma-Aldrich 203637) for 12 hours before measuring luminescence to stimulate β-catenin transcriptional activity. For NFATc3 luciferase experiments, HeLa cells were transfected with 0.5 μg of plasmid encoding NFATc3 to stimulate transcriptional activity (pBS mNFATc3-EE, Addgene plasmid #17868). Cells were lysed, and luciferase activities were measured using the Dual-Glo luciferase kit (Promega E2920) and a microplate luminometer (BioTek Instruments). Lysates (75 μL) were pipetted into 96-well plates in triplicate. Data were calculated as luciferase/Renilla signal. Fold change was calculated based on change from unstimulated baseline (e.g., LiCl treated vs untreated or NFATc3 transfected vs control transfected).

Animal studies

Animal and experimental protocols

Transgenic human-V5-DNAJB6b mice with *MCK* promoter were previously generated.[8] DNAJB6b-F93L mice develop a prominent myopathy and are weak by age 3 months.[8] Mice were housed in a temperature-controlled environment with 12-hour light-dark cycles and received food and water ad libitum. Mice were killed, and skeletal muscle was dissected. For western blot analysis, muscle was flash frozen in liquid nitrogen and stored at −80°C.

Wire screen holding and grip test

Grip strength testing consisted of 5 separate measurements using a trapeze bar attached to a force transducer that recorded peak-

Figure 1 DNAJB6 knockout results in accumulation of sarcomeric proteins and altered myofibrillogenesis
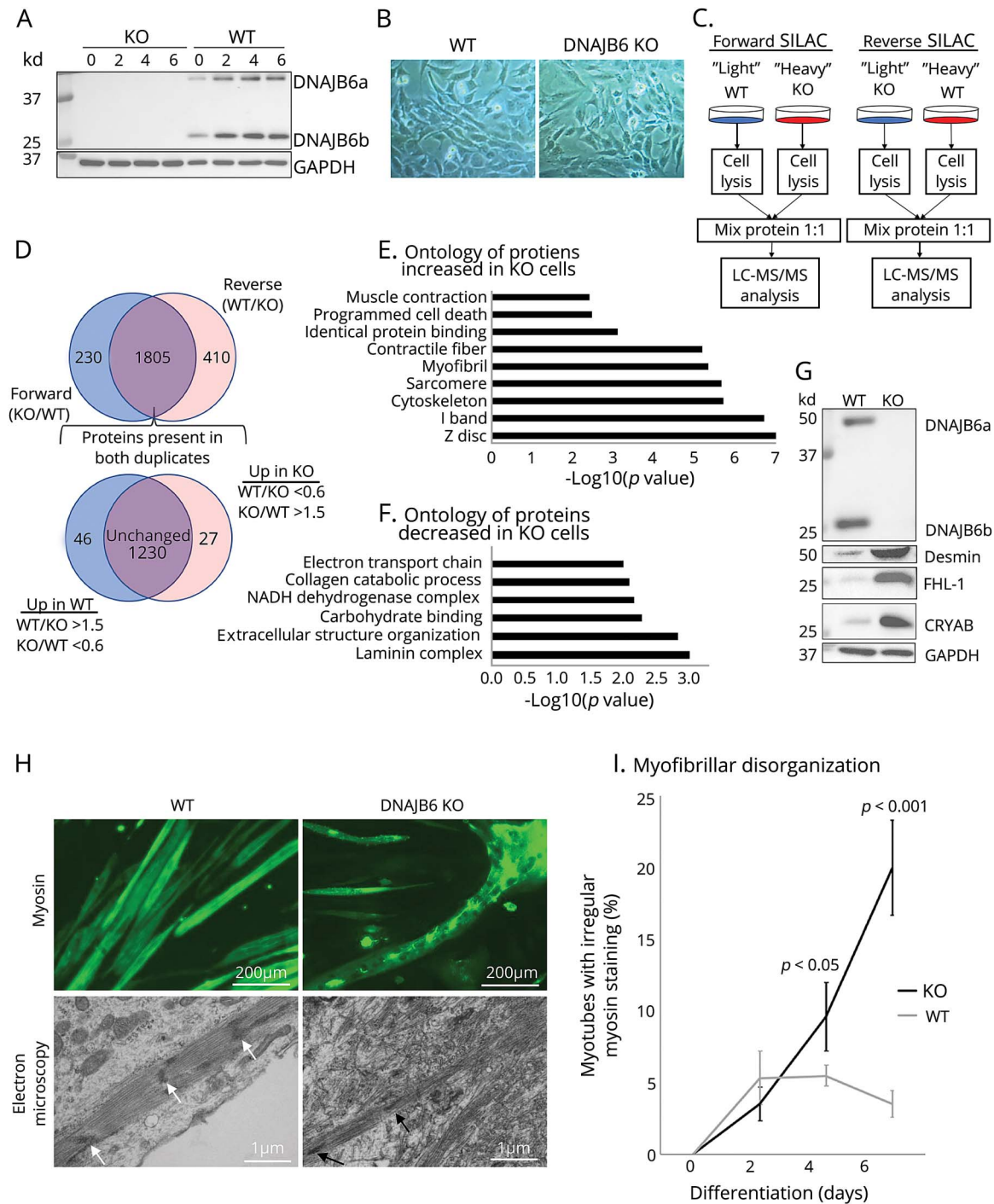
(A) Western blot demonstrating the absence of both DNAJB6 isoforms in Crispr/Cas9-generated DNAJB6 KO C2C12 myoblasts and during differentiation into myotubes. (B) Bright-field image demonstrating normal morphology of DNAJB6 KO myoblasts. (C) Flowchart of forward and reverse SILAC labeling combined with LC-MS/MS for comparative analysis of protein expression in WT and DNAJB6 KO myoblasts. (D) Quantitation overlap of the detected proteins in the 2 forward and 2 reverse SILAC labeling experiments and those that differentially accumulated in WT vs DNAJB6 KO C2C12 cells. (E) Ontological analysis of proteins increased in DNAJB6 KO myoblasts. (F) Ontological analysis of proteins decreased in DNAJB6 KO myoblasts. (G) Western blot of WT and KO myoblasts confirming increased levels of several proteins identified in SILAC analysis. (H) Differentiation of KO myoblasts into myotubes reveals altered myofibrillar organization on myosin staining and electron microscopy. White arrows demonstrate Z discs in WT myotubes with well-organized sarcomeres. Dark arrows demonstrate Z discs in KO myotubes with poor myofibrillar organization. (I) Quantitation of myotubes with irregular myosin staining. Error bars represent the standard error of 3 independent experiments. KO = knockout; LC-MS/MS = liquid chromatography with tandem mass spectrometry; SILAC = stable isotope labeling with amino acids in cell culture; WT = wild type.

Table Increased proteins in DNAJB6 KO myoblasts

Gene	Protein	KO/WT average
PDLIM3	**PDZ and LIM domain protein 3**	**6.89**
PTGIS	Prostacyclin synthase	4.30
ACTN3	**Alpha-actinin-3**	**4.22**
SERPINB9B	Serpin B9	3.99
TPPP3	Tubulin polymerization-promoting protein family member 3	3.30
FTL1	Ferritin light chain 1	3.24
NAPA	Alpha-soluble NSF attachment protein	3.16
CRYAB	**Alpha-crystallin B chain**	**3.00**
AKAP12	**Isoform 2 of A-kinase anchor protein 12**	**2.92**
RPL14	60S ribosomal protein L14	2.69
EXOC1	Exocyst complex component 1	2.42
FHL1	**Four and a half LIM domains protein 1**	**2.34**
SGPL1	Sphingosine-1-phosphate lyase 1	2.26
JUP	**Junction plakoglobin**	**2.18**
PAK2	Serine/threonine protein kinase PAK 2	2.13
DNM1L	Isoform 4 of dynamin-1-like protein	2.09
DES	**Desmin**	**2.05**
TUBB3	Tubulin beta-3 chain	1.97
GAA	Lysosomal alpha-glucosidase	1.96
UGP2	Isoform 2 of UTP—glucose-1-phosphate uridylyltransferase	1.95
CTSL	Cathepsin L1	1.86
DNAJB4	**DnaJ homolog subfamily B member 4**	**1.83**
HSPB1	**Isoform B of heat shock protein beta-1**	**1.82**
MVP	Major vault protein	1.81
ABRACL	Costars family protein ABRACL	1.80
PDLIM1	**PDZ and LIM domain protein 1**	**1.78**
KLC2	Kinesin light chain 2	1.75

Abbreviations: KO = knockout; SILAC = stable isotope labeling with amino acids in cell culture; WT = wild type.
Note the many sarcomeric and chaperone proteins increased in DNAJB6 KO myoblasts (* and bold). Proteins meeting SILAC threshold of KO/WT ratio of >1.5 and WT/KO ratio of <0.6.

generated force while mice were pulled backward by their tail (Stoelting, Wood Dale, IL). The resulting measurement was recorded, and the average of the highest 3 measurements was determined to give the strength score. Another quantitative strength measurement was performed by wire screen holding test. Mice were placed on a grid where it stood using all 4 limbs. Subsequently, the grid was inverted 15 cm above a cage. Latency for the mouse to release the mesh is recorded, and the average hanging time of 3 trials was used.

Histochemistry

Isolated muscle was mounted using tragacanth gum (Sigma, G1128) and quick frozen in liquid nitrogen–cooled 2-methylbutane. Samples were stored at −80°C until sectioning into 10-μm sections. Hematoxylin and eosin staining was performed as previously described.[19] Images were taken with a 5-megapixel color charge coupled device (Nikon, Tokyo, Japan), and the muscle fiber cross-sectional area (CSA) was measured using ImageJ software. Two separate individuals, blinded to the treatment status of mice, took photographs and measured the CSA. Four representative images from each animal's tibialis anterior were used to determine the average cross-sectional area.

Lithium treatment

After oxygen exposure, mice were anesthetized with isofluorane and injected intraperitoneally with LiCl (250 mg/kg body weight; Sigma-Aldrich) or dimethyl sulfoxide daily for 1 month.

Statistical analysis

Results are presented as mean and standard error of the mean. Statistical analyses were performed using paired t tests.

Standard protocol approvals, registrations, and patient consents

All animal experimental protocols were approved by the Animal Studies Committee of Washington University School of Medicine.

Data availability policy

The supplementary data can be accessed via links.lww.com/NXG/A145 and links.lww.com/NXG/A147. The authors will share the data of this study by request from any qualified investigator. Any data not published within the article are available in a public repository and will be shared by request from any qualified investigator.

Results

DNAJB6 KO myoblasts accumulate sarcomeric proteins and form altered myofibrillar structures

To understand DNAJB6's role in skeletal muscle, we generated C2C12 myoblasts that lack both isoforms of DNAJB6 (DNAJB6a and DNAJB6b) using CRISPR/cas9 technology (figure 1A). These undifferentiated cells were viable and morphologically similar to control C2C12 cells (figure 1B). To identify differentially accumulated proteins, we performed SILAC. SILAC experiments were conducted in duplicate, including 2 forward (KO/WT) and 2 reverse labeling (WT/KO) of control and DNAJB6 KO C2C12 myoblasts (figure 1C depicts the setup for SILAC-based proteomics). Using

Figure 2 Absence of DNAJB6 impairs GSK3β dephosphorylation and enhances myotube formation
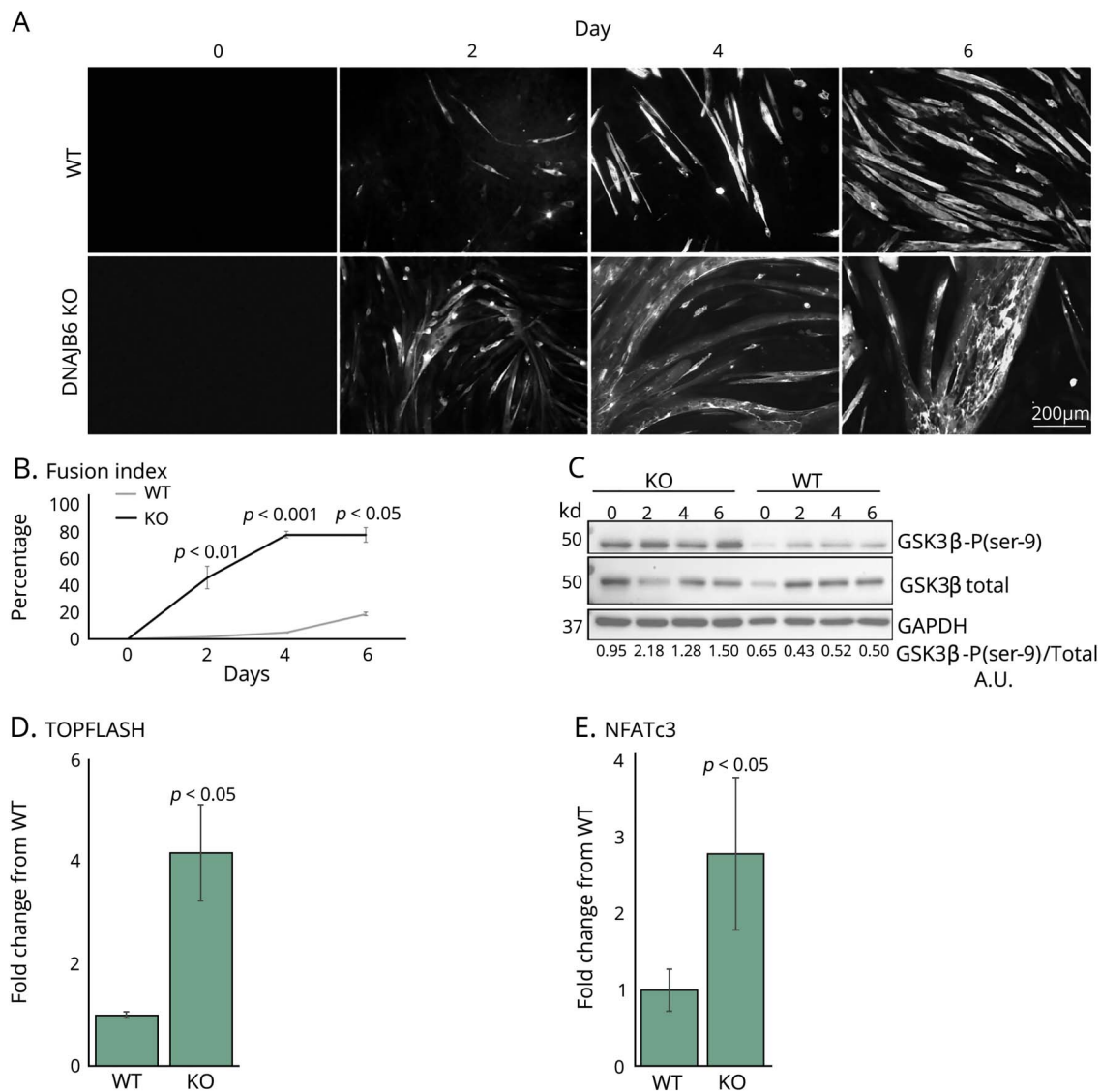

(A) C2C12 WT and DNAJB6 KO myoblasts differentiated into myotubes for 6 days and stained for myosin. DNAJB6 KO myoblasts fused to form large myotubes with enhanced fusion index (B). Error bars represent the standard error of 3 independent experiments. (C) Western blot confirmed increased inactive GSK3β-P(ser-9) in KO myoblasts. GSK3β-P(ser-9)/GSK3β-total ratio is given below western blot. (D) Increased β-catenin transcriptional activity in DNAJB6 KO myoblasts compared with WT myoblasts measured by TOPFLASH luciferase assay. (E) Increased NFATc3 transcriptional activity in DNAJB6 KO myoblasts compared with WT myoblasts. Error bars represent the standard error of at least 2 independent experiments. GSK3β = glycogen synthase kinase-β; KO = knockout; NFATc3 = nuclear factor of activated T cells cytoplasmic 3; WT = wild type.

liquid chromatography with tandem mass spectrometry analysis, we quantified 2035 proteins in the 2 forward experiments, 2215 proteins in the 2 reverse experiments, and a total of 2445 distinct proteins overall (figure 1D). Nearly 75% of the proteins quantified were present in both forward and reverse experiments (figure 1D). For subsequent data analysis, we used only proteins present in both duplicates of the forward and reverse experiments (figure 1D). To identify proteins that accumulate in DNAJB6 KO cells, we used 2 thresholds: a 1.5-fold change in forward KO/WT experiments and a 0.6-fold change in reverse WT/KO experiments. Based on these criteria, 27 proteins were identified (figure 1D, table

1). Ontological analysis of the 27 proteins increased in KO cells identified categories such as sarcomere, Z disc, and muscle contraction (figure 1E). Notably, these proteins included several Z-disc proteins such as desmin, α-actinin, FHL-1, and PDZ-Lim domain proteins 1 and 3. It also identified the co-chaperone DNAJB4 and small HSPs HSPB1 and HSPB5 (αβ-crystallin). Reversal of thresholds to identify proteins decreased in DNAJB6 KO cells identified 46 proteins belonging to several ontological categories including laminin complex and collagen catabolic process (figure 1, D and F, table e-1, links.lww.com/NXG/A145). Immunoblotting of lysates from control and DNAJB6 KO
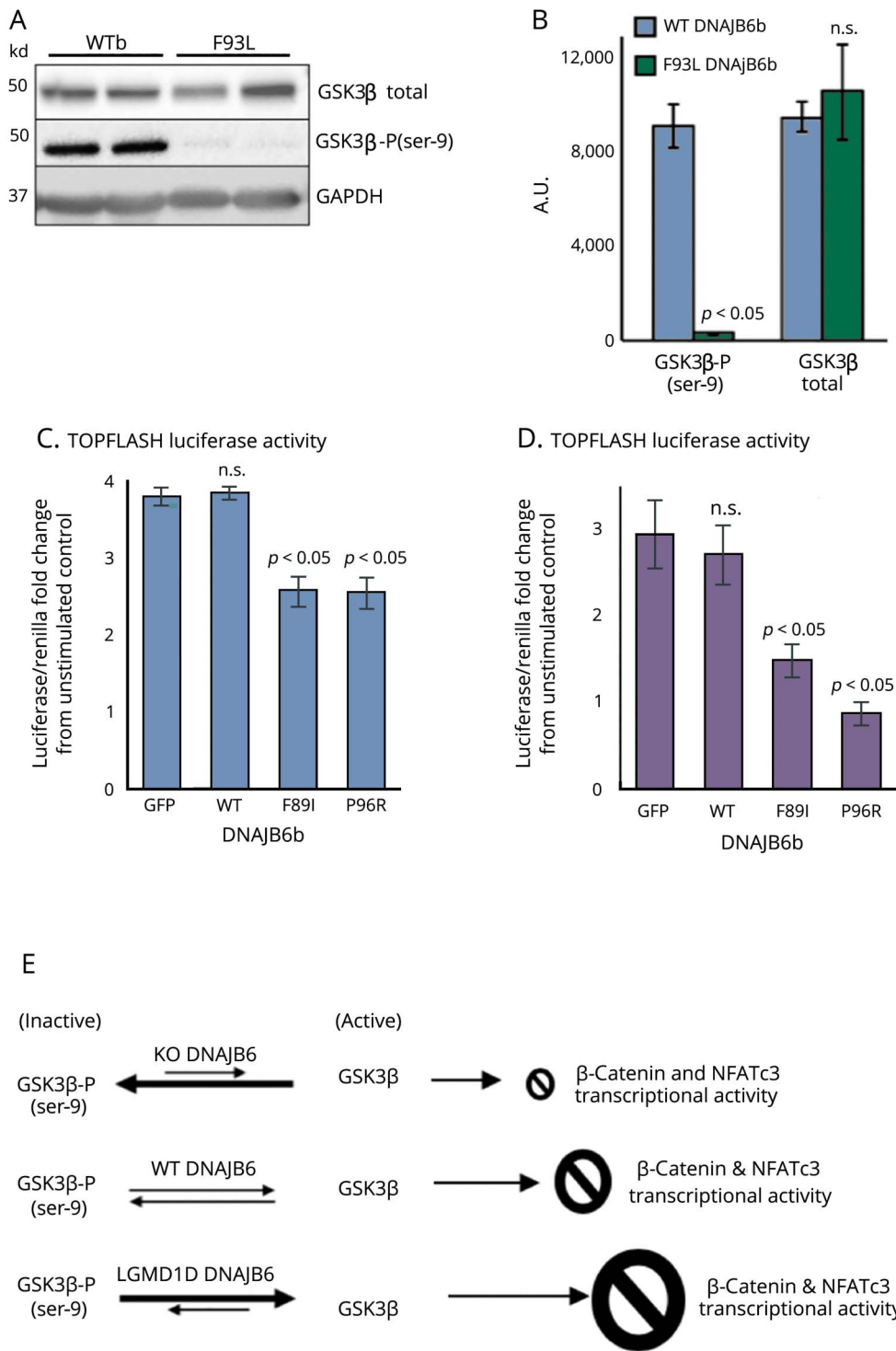
(A) Western blot of skeletal muscle lysates from 3-month old LGMD1D mutant mice (F93Lb, n = 2) vs control (WTb, n = 2) demonstrating significantly reduced inactive GSK3β-P(ser-9) in mutant mice. Error bars represent the standard error. (B) Quantitation of western blot. Dual-luciferase assay demonstrating reduced β-catenin (C) and NFATc3 (D) transcriptional activity in HeLa cells transfected with mutant DNAJB6b constructs compared with unstimulated controls. β-catenin transcriptional activity was stimulated via treatment with 20 mM LiCl for 12 hours. NFATc3 transcriptional activity was stimulated by overexpression of NFATc3 via transient transection. Error bars in C and D represent the standard error from 3 separate experiments. (E) Proposed model for DNAJB6's spectrum of impact on GSK3β activation and myogenesis. GSK3β = glycogen synthase kinase-β; LGMD1D = limb-girdle muscular dystrophy 1D; NFATc3 = nuclear factor of activated T cells cytoplasmic 3; WT = wild type.

myoblasts for several of these proteins confirmed their accumulation (figure 1G). Skeletal muscle from LGMD1D mice similarly demonstrates an accumulation of several of these Z-disc proteins.[8] When differentiated into myotubes, DNAJB6 KO cells contained abnormal myofibrillar structures characterized by irregular myosin immunofluorescence and disorganized sarcomere organization on electron microscopy (figure 1, H and I). Overall, this suggests that the absence of DNAJB6 leads to impaired organization and accumulation of sarcomeric proteins. These findings are similar to the myofibrillar abnormalities noted in mouse and human LGMD1D skeletal muscle.[3,8]

Figure 4 GSK3β inhibition improves muscle strength in LGMD1D mice
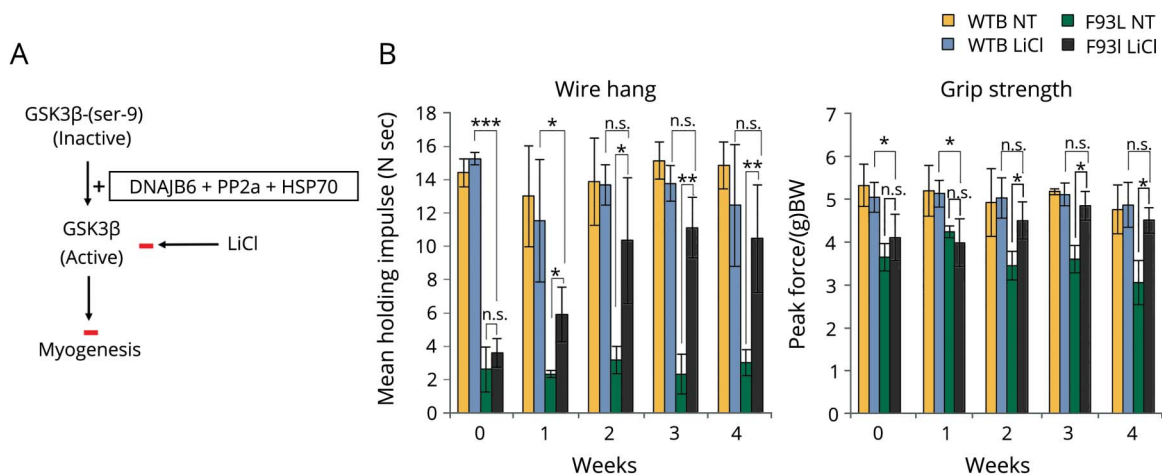
(A) Diagram demonstrating DNAJB6's role in chaperoning the dephosphorylation of GSK3β-P(ser-9) and treatment strategy with GSK3β inhibitor, LiCl. (B) Functional testing (wire hang and grip strength) of 3-month-old DNAJ6b-WT and DNAJB6b-F93L mice treated daily with LiCl vs no treatment (NT). Two independent experiments were performed for a total of 8 mice per condition. Strength of DNAJB6b-F93L mice treated with LiCl significantly improves over the course of the month and reaches levels similar to DNAJB6b-WT mice. Error bars represent the standard error. *$p < 0.05$, **$p < 0.01$, ***$p < 0.005$. GSK3β = glycogen synthase kinase-β; WT = wild type.

KO of DNAJB6 in myoblasts impairs GSK3β activation and enhances myogenesis

When differentiated for 6 days, C2C12 myoblasts form myotubes with a fusion index (nuclei contained in myotubes/total nuclei) of approximately 20% (figure 2, A and B). Surprisingly, we found that DNAJB6 KO myotubes have an enhanced fusion index (77%) and form enlarged myotubes (figure 2, A and B). This suggested that DNAJB6 may play a role in myogenic signaling pathways. DNAJB6 is known to chaperone the dephosphorylation (activation) of GSK3β, an important signaling kinase that suppresses several myogenic signaling pathways.[10,14,15,20] Compared with WT, DNAJB6 KO myoblasts and myotubes contained increased levels of phosphorylated (inactive) GSK3β-P(ser-9) (figure 2C). This suggests that the absence of DNAJB6 is associated with impaired GSK3β-P(ser-9) dephosphorylation and supports DNAJB6's proposed role in GSK3β activation.[10] GSK3β's impact on myogenesis is thought to be mediated through suppression of β-catenin and NFATc3 signaling.[13–15] We therefore evaluated β-catenin and NFATc3 transcriptional activity using dual luciferase assays. We found that both NFATc3 and β-catenin transcriptional activity were increased in DNAJB6 KO myoblasts (figure 2, D and E). These findings suggest that the enlarged myotubes and enhanced fusion index resulting from loss of DNAJB6 may be related to impaired GSK3β-P(ser-9) dephosphorylation and increased β-catenin and NFATc3 transcriptional activity.

LGMD1D mutations enhance GSK3β dephosphorylation in skeletal muscle

We next investigated the impact of dominant *DNAJB6* disease-causing mutations on GSK3β's phosphorylation

state in muscle. We used skeletal muscle lysate from 3-month-old LGMD1D model mice that express a V5-tagged DNAJB6b-F93L transgene and control mice that express a DNAJB6b-WT transgene.[8] Of interest, we found a near complete absence of GSK3β-P(ser-9) in the LGMD1D mice (figure 3, A and B). This suggested that *DNAJB6* disease mutations increase GSK3β dephosphorylation to its active state. We next evaluated the impact of *DNAJB6* mutations on myogenic signaling pathways downstream of GSK3β. We used a dual luciferase assay to measure β-catenin and NFATc3 transcriptional activity in HeLa cells transfected with GFP-tagged DNAJB6 constructs. We treated cells with 20 mM LiCl, a GSK3β inhibitor, to stimulate β-catenin transcriptional activity (figure 3C). We overexpressed NFATc3 via transient transfection of cells to stimulate NFATc3 transcriptional activity. We found that both β-catenin and NFATc3 transcriptional activity were suppressed by the presence of various DNAJB6 mutants (figure 3, C and D).

These findings illustrate DNAJB6's spectrum of impact on GSK3β's activity: absence of DNAJB6 is associated with impaired dephosphorylation of GSK3β-P(ser-9), whereas dominant disease-causing mutations in *DNAJB6* enhance dephosphorylation GSK3β-P(ser-9) to its active form (figure 3E).

GSK3β inhibitor LiCl improves strength, muscle mass, and histopathology in LGMD1D mice

To test the therapeutic potential of GSK3β inhibition (figure 4A), we treated 3-month-old control mice overexpressing DNAJB6b-WT and mutant mice overexpressing DNAJB6b-F93L with either vehicle (dimethyl sulfoxide) or LiCl via

Figure 5 GSK3β inhibition improves muscle size in LGMD1D mice
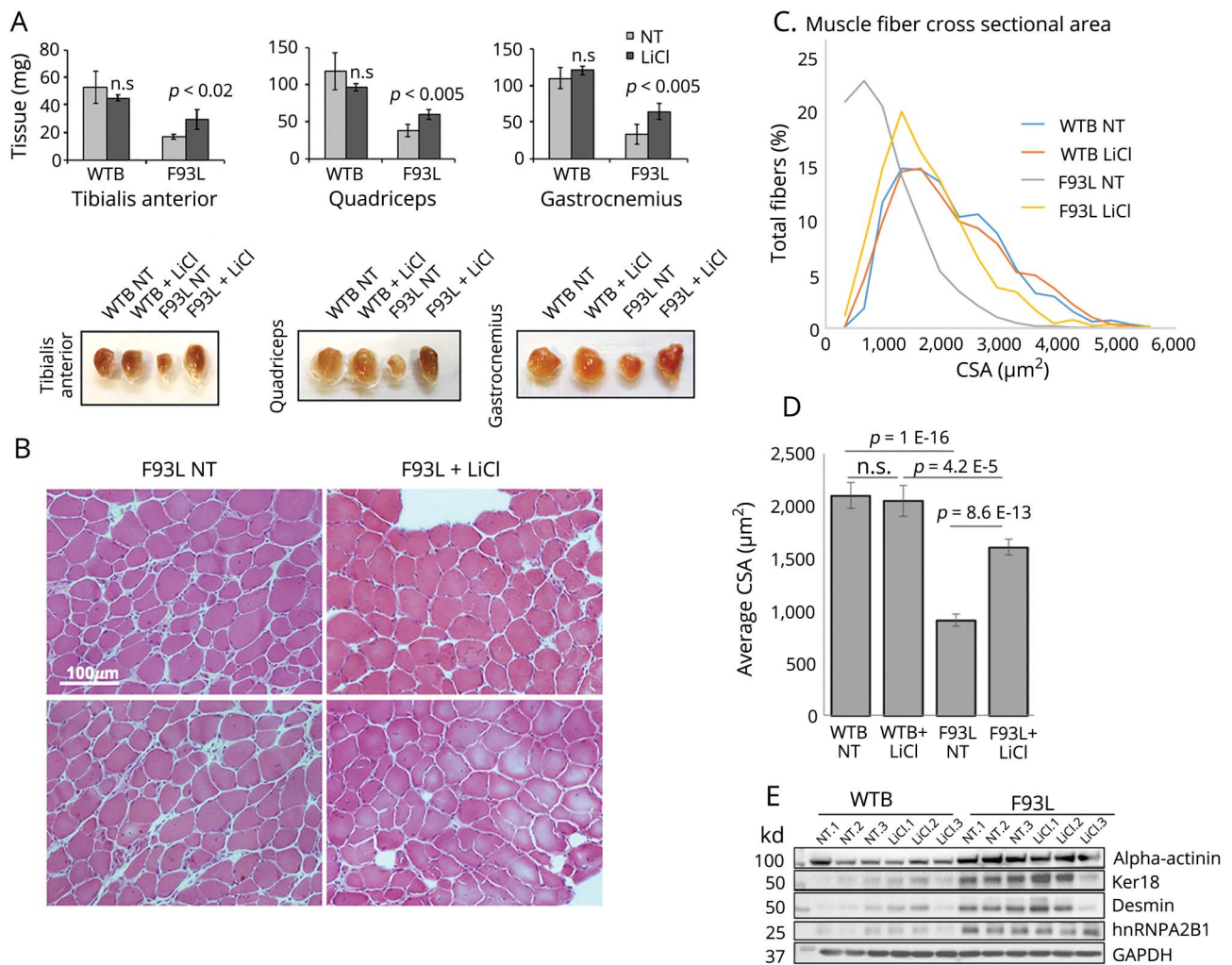
(A) Mass of selected muscles after 1 month of treatment. Note visible difference in the size of F93L muscles treated with LiCl. (B) H&E staining of TA from LiCl treated or untreated F93L mice illustrating increased muscle fiber size and reduced fiber size variability. Two representative examples are provided from the tibialis anterior. (C) Quantitation of fiber CSA profile demonstrates an overall increase in the muscle fiber size after LiCl treatment in F93L mice and no change in LiCl-treated control mice. (D) Average muscle fiber cross-sectional area of LiCl-treated F93L mice significantly improves but does not reach control levels. LiCl does not alter the muscle fiber size of control mice. Error bars from A and D represent the standard error. (E) Western blot of skeletal muscle lysates in LiCl-treated and untreated mice illustrates no improvement in accumulated sarcomeric proteins or RNA-binding proteins in F93L mice. WT = wild type.

daily intraperitoneal injection for 1 month. Results were obtained from 4 mice per group. Two independent experiments were performed for a total of 8 mice per condition. We used a dose of 250 mg/kg body weight to mimic therapeutic serum levels in humans.[21,22] Skeletal muscle function of LiCl-treated DNAJB6b-F93L mice, as measured by grip strength and inverted wire hang test, normalized to that of control mice over the course of the month (figure 4B). The mass and visible size of selected muscles and muscle fiber CSA were significantly increased in DNAJB6b-F93L mice treated with LiCl (figure 5, A-D). Despite improvements in strength and muscle fiber size, western blot analyses of skeletal muscle lysates demonstrated no change in accumulated sarcomeric proteins or RNA-binding proteins seen with *DNAJB6* mutations (figure 5E).

Discussion

This study demonstrates that DNAJB6's role in skeletal muscle involves not only sarcomeric protein quality control but also suppression of myogenic signaling pathways important for myoblast differentiation, myotube fusion, skeletal muscle hypertrophy, and regeneration. Many other skeletal muscle chaperones also have dual roles in protein quality control and modulation of signaling pathways. The co-chaperone BAG3 facilitates autophagic sorting of damaged filamin to lysosomes while also engaging in YAP/TAZ mechanotransduction signaling.[23] αB-crystallin not only functions as a desmin chaperone at the Z disc but also modulates NF-κβ and TGF-β2 signaling.[24,25] HSP70 and HSP90 not only play key roles in myofibrillogenesis but also act

as circulating cachexins by activating the p38β-MAPK-C/EBPβ catabolic signaling pathway.[26] Although these dual functions may initially seem unrelated, regulation of protein synthesis is central to both these stress signaling pathways and maintaining balanced protein homeostasis. It is therefore not surprising to find chaperones that coordinate protein quality control with signaling pathways regulating protein synthesis.

Our comparisons between DNAJB6 KO and dominant LGMD1D models facilitated many interesting observations of DNAJB6's dual roles in skeletal muscle. For instance, KO of DNAJB6 in myoblasts and myotubes recapitulated the myofibrillar disorganization and accumulation of sarcomeric proteins seen in LGMD1D patients and animal models.[3,8] In general, protein aggregation in myopathies may occur from mutations causing a protein itself to misfold and aggregate (e.g., desmin) or from mutations in protein quality control machinery (e.g., αβ-crystallin) causing other proteins to aggregate (desmin). With DNAJB6, the absence of sarcomeric chaperone activity could explain the altered myofibrillar assembly and accumulation of sarcomeric proteins in KO cells. Other DNAJB6 KO models have similarly resulted in aggregation of client proteins.[27,28] Because LGMD1D is not due to a KO or loss of DNAJB6, one could speculate that the vacuolar and aggregate myopathology seen with disease mutations results from a dominant negative effect on DNAJB6's sarcomeric chaperone activities. Lending support to this theory, mutations in *VCP*, *BAG3*, and *CRYAB* are also thought to cause myopathies with vacuoles and aggregates from a dominant negative mechanism.[29–31]

However, several findings in this study do not fit this theory. Specifically, dominant mutations and absence of DNAJB6 had opposite effects on GSK3β phosphorylation status and downstream myogenic signaling pathways. We found an increased size of DNAJB6 KO myotubes owing to an enhanced fusion index. This may be related to impaired dephosphorylation of GSK3β-P(ser-9) and derepression of downstream myogenic signaling pathways such as β-catenin and NFATc3.[9–12,32] Contrary to KO cells, dominant *DNAJB6* mutations were associated with an enhanced dephosphorylation of GSK3β-P(ser-9) and suppressed β-catenin and NFATc3 transcriptional activity. Although DNAJB6 is known to chaperone the dephosphorylation of GSK3β-P(ser-9) to maintain it in an active state, the exact mechanism linking *DNAJB6* disease mutations with enhanced GSK3β-P(ser-9) dephosphorylation is not clear. One could speculate that it may be related to a gain of function from increased stability of the mutant DNAJB6 protein; however, further studies are needed.[4,8]

As DNAJB6 appears to have multiple functions within skeletal muscle, it is not surprising that mutations may cause disease through multiple mechanisms. LiCl is well suited to address alterations in both GSK3β signaling and protein aggregation. It acts as a competitive inhibitor of the adenosine triphosphate–magnesium-dependent catalytic activity of GSK3β and may also act indirectly through enhanced phosphorylation of GSK3β.[33] Although GSK3β activity suppresses myogenesis and blunts skeletal muscle regeneration, it has also been linked to formation of aggregates in several disorders, making GSK3β inhibition a good strategy for LGMD1D treatment.[34,35] LiCl also stimulates autophagy independent of GSK3β, which may benefit LGMD1D further.[36] Given LiCl's dual impact on GSK3β and autophagy, many have used it to treat in vivo models of neurologic disorders with protein aggregate pathology and GSK3β dysfunction, such as Huntington disease, Alzheimer disease, *SOD1* amyotrophic lateral sclerosis, Parkinson disease, and inclusion body myositis.[33–35,37–40] In addition to showing therapeutic efficacy in these animal models, LiCl improved biochemical markers of disease and histopathologic evidence of aggregates.[34,37–40] These previous studies raise the possibility that the significant improvement of LGMD1D mice treated with LiCl was due to enhanced autophagy and clearance of accumulated sarcomeric proteins. Of interest, the accumulations of sarcomeric and RNA binding proteins in mutant mouse muscle were not altered by LiCl treatment (figure 5E). This lack of improvement may simply be due to pathologic changes lagging behind functional improvements. However, it may actually suggest that LGMD1D pathogenesis is due not only to DNAJB6 dysfunction in protein quality control but also to GSK3β-related signaling pathways. Further studies are required to clarify, however, that LiCl may be an ideal therapeutic option for LGMD1D.

Disclosure

A.R. Findlay has received foundation/society research support from the American Academy of Neurology. R. Bengoechea has served on the editorial board of *BioMed Central Neuroscience*. S.K. Pittman reports no disclosures. T.-F. Chou has served on the editorial board of the *Journal of Cancer Sciences*; holds patents in Methods and Compositions for Inhibition of the Transitional Endoplasmic Reticulum ATPase; and has received government funding from the NIH. H.L. True has served on the editorial board of *PLOS Pathogens* and has received government funding from the NIH. C.C. Weihl has served on advisory boards of Novartis, Acceleron, and Sarepta; has served on the editorial board of *Neuromuscular Disorders*; has received government funding from the NIH; and has received foundation/society research support from the Muscular Dystrophy Association and the Myositis Association. Disclosures available: Neurology.org/NG.

Appendix Author contributions

Name	Location	Role	Contribution
Andrew R. Findlay, MD	Washington University St. Louis	Author	Design and conceptualization of the study, acquisition of data, interpretation of data, writing of the manuscript, and revision of the manuscript for intellectual content.
Rocio Bengoechea, PhD	Washington University St. Louis	Author	Acquisition of data and revision of the manuscript for intellectual content.
Sara K. Pittman, BS	Washington University St. Louis	Author	Acquisition of data.
Tsui-Fen Chou, PhD	Harbor-UCLA Medical Center	Author	Acquisition of data, interpretation of data, and revision of the manuscript for intellectual content.
Heather L. True, PhD	Washington University St. Louis	Author	Revision of the manuscript for intellectual content.
Conrad C. Weihl, MD, PhD	Washington University St. Louis	Author	Design and conceptualization of the study, interpretation of data, and revision of the manuscript for intellectual content.

References

1. Smith DA, Carland CR, Guo Y, Bernstein SI. Getting folded: chaperone proteins in muscle development, maintenance and disease. Anat Rec (Hoboken) 2014;297:1637–1649.
2. Harms MB, Sommerville RB, Allred P, et al. Exome sequencing reveals DNAJB6 mutations in dominantly-inherited myopathy. Ann Neurol 2012;71:407–416.
3. Sandell S, Huovinen S, Palmio J, et al. Diagnostically important muscle pathology in DNAJB6 mutated LGMD1D. Acta Neuropathol Commun 2016;4:9.
4. Sarparanta J, Jonson PH, Golzio C, et al. Mutations affecting the cytoplasmic functions of the co-chaperone DNAJB6 cause limb-girdle muscular dystrophy. Nat Genet 2012;44:450–452, S1–2.
5. Straub V, Murphy A, Udd B. LGMD workshop study group. 229th ENMC international workshop: Limb girdle muscular dystrophies—Nomenclature and reformed classification Naarden, the Netherlands, 17-19 March 2017. Neuromuscul Disord 2018;28:702–710.
6. Kampinga HH, Craig EA. The HSP70 chaperone machinery: J proteins as drivers of functional specificity. Nat Rev Mol Cell Biol 2010;11:579–592.
7. Seki N, Hattori A, Hayashi A, Kozuma S, Miyajima N, Saito T. Cloning, tissue expression, and chromosomal assignment of human MRJ gene for a member of the DNAJ protein family. J Hum Genet 1999;44:185–189.
8. Bengoechea R, Pittman SK, Tuck EP, True HL, Weihl CC. Myofibrillar disruption and RNA-binding protein aggregation in a mouse model of limb-girdle muscular dystrophy 1D. Hum Mol Genet 2015;24:6588–6602.
9. Meng E, Shevde LA, Samant RS. Emerging roles and underlying molecular mechanisms of DNAJB6 in cancer. Oncotarget 2016;7:53984–53996.
10. Mitra A, Menezes ME, Pannell LK, et al. DNAJB6 chaperones PP2A mediated dephosphorylation of GSK3β to downregulate β-catenin transcription target, osteopontin. Oncogene 2012;31:4472–4483.
11. Mitra A, Menezes ME, Shevde LA, Samant RS. DNAJB6 induces degradation of beta-catenin and causes partial reversal of mesenchymal phenotype. J Biol Chem 2010;285:24686–24694.
12. Menezes ME, Mitra A, Shevde LA, Samant RS. DNAJB6 governs a novel regulatory loop determining Wnt/β-catenin signalling activity. Biochem J 2012;444:573–580.
13. Suzuki A, Pelikan RC, Iwata J. WNT/β-Catenin signaling regulates multiple steps of myogenesis by regulating step-specific targets. Mol Cell Biol 2015;35:1763–1776.
14. van der Velden JL, Schols AM, Willems J, Kelders MC, Langen RC. Glycogen synthase kinase 3 suppresses myogenic differentiation through negative regulation of NFATc3. J Biol Chem 2008;283:358–366.
15. Vyas DR, Spangenburg EE, Abraha TW, Childs TE, Booth FW. GSK-3beta negatively regulates skeletal myotube hypertrophy. Am J Physiol Cell Physiol 2002;283:C545–C551.
16. Dai YS, Xu J, Molkentin JD. The DnaJ-related factor Mrj interacts with nuclear factor of activated T cells c3 and mediates transcriptional repression through class II histone deacetylase recruitment. Mol Cell Biol 2005;25:9936–9948.
17. Kato M, Chou TF, Yu CZ, DeModena J, Sternberg PW. LINKIN, a new transmembrane protein necessary for cell adhesion. Elife 2014;3:e04449.
18. Sapir A, Tsur A, Koorman T, et al. Controlled sumoylation of the mevalonate pathway enzyme HMGS-1 regulates metabolism during aging. Proc Natl Acad Sci USA 2014;111:E3880–E3889.
19. Kim HJ, Kim NC, Wang YD, et al. Mutations in prion-like domains in hnRNPA2B1 and hnRNPA1 cause multisystem proteinopathy and ALS. Nature 2013;495:467–473.
20. Pansters NA, Schols AM, Verhees KJ, et al. Muscle-specific GSK-3β ablation accelerates regeneration of disuse-atrophied skeletal muscle. Biochim Biophys Acta 2015;1852:490–506.
21. Patel NC, DelBello MP, Bryan HS, et al. Open-label lithium for the treatment of adolescents with bipolar depression. J Am Acad Child Adolesc Psychiatry 2006;45:289–297.
22. Nair AB, Jacob S. A simple practice guide for dose conversion between animals and human. J Basic Clin Pharm 2016;7:27–31.
23. Ulbricht A, Eppler FJ, Tapia VE, et al. Cellular mechanotransduction relies on tension-induced and chaperone-assisted autophagy. Curr Biol 2013;23:430–435.
24. Adhikari AS, Singh BN, Rao KS, Rao CM. αB-crystallin, a small heat shock protein, modulates NF-κB activity in a phosphorylation-dependent manner and protects muscle myoblasts from TNF-α induced cytotoxicity. Biochim Biophys 2011;1813:1532–1542.
25. Nahomi RB, Pantcheva M, Nagaraj RH. αB-Crystallin is Essential for the TGF-β2-mediated Epithelial to Mesenchymal Transition of Lens Epithelial Cells. Biochem J 2016;473:1455–1469.
26. Zhang G, Liu Z, Ding H, et al. Tumor induces muscle wasting in mice through releasing extracellular Hsp70 and Hsp90. Nat Commun 2017;8:589.
27. Watson ED, Geary-Joo C, Hughes M, Cross JC. The Mrj co-chaperone mediates keratin turnover and prevents the formation of toxic inclusion bodies in trophoblast cells of the placenta. Development 2007;134:1809–1817.
28. Aprile FA, Källstig E, Limorenko G, Vendruscolo M, Ron D, Hansen C. The molecular chaperones DNAJB6 and Hsp70 cooperate to suppress α-synuclein aggregation. Sci Rep 2017;7:9039.
29. Kitami MI, Kitami T, Nagahama M, et al. Dominant-negative effect of mutant valosin-containing protein in aggresome formation. FEBS Lett 2006;580:474–478.
30. Myers VD, McClung JM, Wang J, et al. The multifunctional protein BAG3: A novel therapeutic target in cardiovascular disease. JACC Basic Transl Sci 2018;3:122–131.
31. Selcen D, Engel AG. Myofibrillar myopathy caused by novel dominant negative αB-crystallin mutations. Ann Neurol 2003;54:804–810.
32. Mitra A, Fillmore RA, Metge BJ, et al. Large isoform of MRJ (DNAJB6) reduces malignant activity of breast cancer. Breast Cancer Res 2008;10:R22.
33. Chuang DM, Wang Z, Chiu CT. GSK-3 as a target for lithium-induced neuroprotection against excitotoxicity in neuronal cultures and animal models of ischemic stroke. Front Mol Neurosci 2011;4:15.
34. Kitazawa M, Trinh DN, LaFerla FM. Inflammation induces tau pathology in inclusion body myositis model via glycogen synthase kinase-3β. Ann Neurol 2008;64:15–24.
35. Beurel E, Grieco SF, Jope RS. Glycogen synthase kinase-3 (GSK3): regulation, actions, and diseases. Pharmacol Ther 2015;148:114–131.
36. Motoi Y, Shimada K, Ishiguro K, Hattori N. Lithium and autophagy. ACS Chem Neurosci 2014;5:434–442.
37. Pouladi MA, Brillaud E, Xie Y, et al. NP03, a novel low-dose lithium formulation, is neuroprotective in the YAC128 mouse model of Huntington disease. Neurobiol Dis 2012;48:282–289.
38. Zhang X, Heng X, Li T, et al. Long-term treatment with lithium alleviates memory deficits and reduces amyloid-β production in an aged Alzheimer's disease transgenic mouse model. J Alzheimers Dis 2011;24:739–749.
39. Fornai F, Longone P, Cafaro L, et al. Lithium delays progression of amyotrophic lateral sclerosis. Proc Natl Acad Sci USA 2008;105:2052–2057.
40. Kim Y-H, Rane A, Lussier S, Andersen JK. Lithium protects against oxidative stress-mediated cell death in α-synuclein-overexpressing in vitro and in vivo models of Parkinson's disease. J Neurosci Res 2011;89:1666–1675.